White Rose Research Online

eprints@whiterose.ac.uk
https://eprints.whiterose.ac.uk
Universities of Leeds, Sheffield and York

Deposited via The University of Leeds.

White Rose Research Online URL for this paper:
https://eprints.whiterose.ac.uk/id/eprint/91819/

Version: Accepted Version

Article:

Streller, F, Agarwal, R, Mangolini, F et al. (2015) Novel Metal Silicide Thin Films by Design via Controlled Solid-State Diffusion. Chemistry of Materials, 27 (12). 4247 - 4253. ISSN: 0897-4756

https://doi.org/10.1021/acs.chemmater.5b01413

Reuse

Items deposited in White Rose Research Online are protected by copyright, with all rights reserved unless indicated otherwise. They may be downloaded and/or printed for private study, or other acts as permitted by national copyright laws. The publisher or other rights holders may allow further reproduction and re-use of the full text version. This is indicated by the licence information on the White Rose Research Online record for the item.

Takedown

If you consider content in White Rose Research Online to be in breach of UK law, please notify us by emailing eprints@whiterose.ac.uk including the URL of the record and the reason for the withdrawal request.

UNIVERSITY OF LEEDS University of Sheffield UNIVERSITY of York

Novel Metal Silicide Thin Films by Design via Controlled Solid-State Diffusion

Frank Streller,[†,§] Rahul Agarwal,[†,§] Filippo Mangolini,[†,∥] and Robert W. Carpick*[,†,‡]

[†]Department of Materials Science and Engineering, University of Pennsylvania, 3231 Walnut Street, Philadelphia, Pennsylvania 19104, United States

[‡]Department of Mechanical Engineering and Applied Mechanics, University of Pennsylvania, 220 S. 33rd Street, Philadelphia, Pennsylvania 19104, United States

ABSTRACT: In the quest to accelerate the discovery and deployment of new materials with ideal and tailored properties, synthesis via solid-state diffusion holds particular promise as it allows the crystal structure and stoichiometry of thin films to be controlled independently of the deposition method. However, the kinetics and the quality of the resulting materials remain relatively unexplored. Here we demonstrate both source-limited and kinetically-limited solid-state diffusion as novel routes to tune the stoichiometry of platinum silicide (Pt_xSi) thin films, representative of metal silicides which have attractive mechanical and electronic properties. Using *in situ* heating inside a transmission electron microscope (TEM) while performing electron diffraction, we show that both routes lead to stoichiometrically-controlled formation of Pt_xSi (x = 1, 2, 3) thin films with high phase selectivity, revealing the crystal structure and formation sequence for each phase. The Pt_xSi formation process from sequentially-deposited layers of platinum (Pt) and amorphous silicon (*a*-Si) significantly differs from the Pt/single-crystal silicon (*sc*-Si) case, allowing the formation of Pt_3Si thin films for the first time.

1. INTRODUCTION

Solid-state reactions to form metal silicides (Me_xSi) have been widely studied since the early 1980s, and were later used for Ohmic contacts, Schottky barrier contacts, gate electrodes, local interconnects, and diffusion barriers in the microelectronics industry.[1−5] Recently, Me_xSi have become attractive as thermoelectric materials due to their metal-like electrical properties combined with semiconductor-like thermal transport.[6−9] Their mechanical robustness and thermal stability makes them promising for high temperature engines,[1] and combined with their high electrical conductivity renders them of interest as next-generation contact materials for nanoelectromechanical (NEM) switches.[10−12] Me_xSi are also considered as alternative plasmonic materials,[13] as well as advanced materials for lithium-ion batteries.[14] One dimensional transition metal silicides have been studied for their exotic properties such as room temperature ferromagnetism and field emission.[15−17] However, most investigations and applications rely on equilibrium Me_xSi phases and do not attempt to control the preceding solid-state diffusion reactions that lead to Me_xSi formation to form specific silicide stoichiometries with desired properties.[18]

Tailoring the physico-chemical properties of Me_xSi through the precise control of their stoichiometry and crystal structure would allow the design of materials suitable for specific applications. Our previous work has shown that the stoichiometry of platinum silicide (Pt_xSi) films greatly influences their electrical conductivity: Pt-rich silicides exhibit metallic-like conductivity, while Si-rich silicides are more resistive.[10,11] Additionally, the nanoscale adhesion of these films to Pt tips decreases from Pt-rich to Si-rich films. To ensure precise stoichiometric control, it is necessary to understand the synthesis mechanism at the atomic scale and the influence of initial precursor concentration in the ensuing chemical transformation. *In situ* TEM experiments have opened up new frontiers for gaining such understanding.[19−23] Here, we use *in situ* TEM to introduce two novel routes to precisely control the stoichiometry of thin Me_xSi films, using Pt_xSi as a model system. In the first, source-limited solid-state diffusion, precise control of the precursor thin film layer thicknesses predetermines the achievable silicide stoichiometry via annealing. In the second, kinetically-limited solid-state diffusion, a precisely controlled time-temperature regime obtains the desired silicide stoichiometry and phase.

2. EXPERIMENTAL SECTION

Samples of different Pt:*a*-Si film thickness ratios were fabricated as precursors to form Pt_xSi films using the source-limited solid-state diffusion approach while assessing their crystal structures and formation sequence. PELCO 50 nm silicon nitride (Si_3N_4) support TEM grids (Ted Pella Inc., Redding, CA) were sputter-coated with thin layers of *a*-Si and Pt, whose thicknesses were chosen to obtain nearly-pure phases of Pt_3Si, Pt_2Si and PtSi upon annealing. The Pt and *a*-Si depositions were conducted sequentially in the same deposition system under maintained vacuum. This minimizes contaminant adsorption between the layers and the oxidation of the *a*-Si - both inhibiting factors for silicidation. The coated grids were removed from the deposition system and characterized using a TEM (JOEL 2100 TEM, JEOL Ltd., Tokyo, Japan).

An *in situ* heating TEM sample holder (Gatan Inc., Pleasanton, CA) was used to anneal the samples in the TEM while continuously recording the electron diffraction pattern (Supporting Information Figure S1), which allowed determination of the crystal structure and formation sequence of the different Pt_xSi phases. All samples were subjected to similar annealing treatments that included a 10 min hold at 500 °C followed by a 10 min hold at 600 °C.

2.1 Film deposition

The Pt and *a*-Si films were sputter deposited in a Denton Vacuum Explorer 14 sputterer (Denton Vacuum Inc, Moorestown, NJ) with a purity of 99.99 % for both films. Pt was deposited in DC mode at 450 W and *a*-Si in AC mode at 230 W. The Pt nanoparticles were produced by coating an *a*-Si film with approx. 10 nm of Pt, which does not wet the surface completely, forming nanoparticles instead of a continuous film.

2.2 Annealing

An *in situ* heating TEM sample holder (Gatan Inc., Pleasanton, CA) was used to form Pt_xSi inside the TEM. The heating holder is equipped with a thermocouple sensitive to ± 1 °C. All source-limited solid-state diffusion samples (*Figure 1* and *Figure 2*) were subject to a similar annealing treatment which included the heating up to 500 °C (heating rate: 30 °C/min) and holding at 500 °C for 10 min. This was followed by heating up to 600 °C (heating rate: 30 °C/min), holding at 600 °C for 10 min and rapid cooling to 50 °C (cooling rate: 85 °C/min). The kinetically-limited solid-state diffusion sample was heated up with a heating rate of 30 °C/min until 200 °C and rapidly quenched to conserve the Pt_3Si phase. Subsequently, the sample was heated up to 300 °C (heating rate: 30 °C/min) to form Pt_2Si followed by rapid quenching. Finally, the sample was heated up to 500 °C (heating rate: 30 °C/min) to form PtSi and subsequently cooled down.

2.3 Transmission electron spectroscopy

All TEM experiments were performed using a JEOL 2100 thermionic emission source TEM (JEOL Ltd., Tokyo, Japan). An accelerating voltage of 200 kV was used with a beam current of 106 μA resulting in a current density of 275 pA/cm^2.

2.4 In situ/ex situ XPS analysis

The chemistry of the near-surface region was investigated by XPS using a customized XPS spectrometer (VG Scienta AB, Uppsala, Sweden)[24]. XPS analyses were performed using a monochromatic Al K_α source (photon energy: 1486.6 eV). The residual pressure in the analysis chamber was constantly less than 1×10^{-8} Torr. The spectrometer was calibrated according to ISO 15472:2001 with an accuracy of ± 0.05 eV. Survey and high-resolution spectra were acquired in constant-analyzer-energy mode with the pass energies of 200 eV and 100 eV, respectively. The full width at half-maximum (FWHM) of the peak-height for the high-resolution Ag $3d_{5/2}$ signal of a sputter-cleaned Ag sample was 0.57 eV. The spectra were processed using CasaXPS software (v.2.3.16, Case Software Ltd., Wilmslow, Cheshire, U.K.). Background subtraction was performed using the Shirley-Sherwood method. The quantitative evaluation of XPS data, as described in [25], was based on integrated intensity using a first-principles model and applying Powell's equation. The inelastic mean free path was calculated using the TPP-2M formula.[26] Curve synthesis for the Pt 4f peaks was performed constraining the integrated intensity ratio of these two signals to 3:4 and their energy separation to 3.33 eV. The reference energies for Pt $4f_{7/2}$ peaks are 71.05 eV, 71.55 eV, 72.18 eV, and 72.75 eV for Pt, Pt_3Si, Pt_2Si, and PtSi respectively.

3. RESULTS AND DISCUSSION

3.1 Source-limited solid-state diffusion

Figure 1 presents the results from the source-limited solid-state diffusion experiments. The Pt:*a*-Si film thickness ratios were chosen to be 1:3 (Pt:*a*-Si=1:3) to form PtSi, 1:1 (Pt:*a*-Si=1:1) for Pt_2Si, and 2:1 (Pt:*a*-Si=2:1) for Pt_3Si. Figure 1a shows representative selected-area electron diffraction (SAD) patterns of an as-deposited Pt/*a*-Si sample and the resulting Pt_xSi film. The diffraction pattern of the as-deposited film (top-right quadrant, Figure 1a) matches the theoretical pattern for Pt (the amorphous structures of the *a*-Si film and Si_3Ni_4 membrane do not produce any diffraction rings). Theoretical diffraction patterns were calculated using the theoretical crystal structures of Pt and Pt_xSi phases and CrystalMaker software (CrystalMaker Software Ltd., Oxfordshire, United Kingdom). For the annealed Pt:*a*-Si=2:1 sample, the 1:1 sample, and the 1:3 sample, the predominant diffraction rings match the theoretical diffraction pattern for monoclinic Pt_3Si (bottom-right quadrant, Figure 1a), tetragonal Pt_2Si (bottom-left quadrant), orthorhombic PtSi (top-left quadrant) respectively. Figure 1b summarizes the formation process of the Pt_3Si, Pt_2Si and PtSi films. The formation process of all three starts with the formation of Pt_3Si. This is the only phase observed for the Pt:*a*-Si=2:1 sample, and was stable throughout the annealing procedure. However, considerable grain-growth occurred with continued heating up to 600 °C as a result of the low Pt_3Si formation temperature of 200 °C, resulting in the appearance of high-intensity diffraction spots (bottom-right quadrant, Figure 1a). For the Pt:*a*-Si=1:1 and Pt:*a*-Si=1:3 samples, Pt_2Si formation followed Pt_3Si formation at approximately 300-325 °C. This phase remained stable for the Pt:*a*-Si=1:1 sample, whereas for the Pt:*a*-Si=1:3 sample, PtSi formed around 400-425 °C.

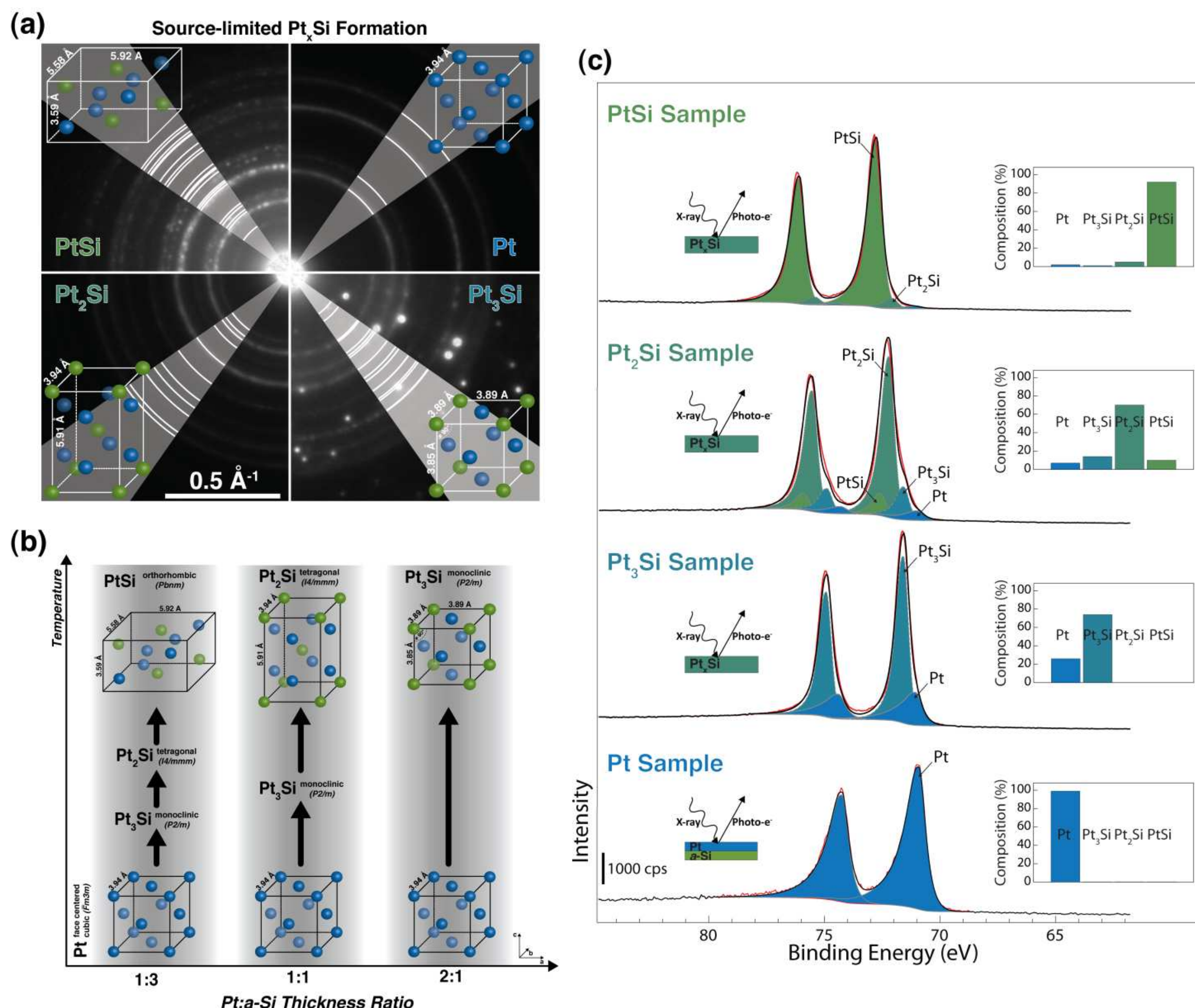

Figure 1. Source-limited Pt_xSi formation. a, Electron diffraction pattern of as-deposited Pt and Pt_3Si, Pt_2Si, and PtSi films produced using source-limited solid-state diffusion. Grey slices indicate diffraction ring positions according to the theoretical crystal structure shown schematically for each phase. b, Schematic of the source-limited solid-state diffusion process which utilizes precise control of the Pt and *a*-Si precursor film thicknesses to predetermine the desired Pt_xSi phase. c, High-resolution XPS spectra of the Pt_4f peaks for as-deposited Pt and resulting Pt_xSi formed on TEM grids using source-limited solid-state diffusion. PtSi sample (Pt:*a*-Si=1:3): quantitative analysis indicates formation of 92% of PtSi. Pt_2Si sample (Pt:*a*-Si=1:1): quantitative analysis indicates formation of 70% Pt_2Si. Pt_3Si sample (Pt:*a*-Si=2:1): quantitative analysis indicates formation of 74% Pt_3Si. Pt sample: quantitative analysis indicates the presence of pure metallic Pt.

The annealed grids were characterized using high-resolution angle-resolved X-ray photoelectron spectroscopy (XPS) to determine the stoichiometry of the films (Figure 1c).[24] In the high-resolution XPS spectrum of as-deposited Pt ("Pt Sample"), the $Pt4f_{7/2}$ peak position (71.05±0.05 eV) and lineshape are characteristic of metallic platinum, thus confirming the TEM diffraction pattern displayed in Figure 1a (top-right quadrant). The high-resolution XPS spectrum of the annealed Pt:*a*-Si=2:1 sample ("Pt_3Si Sample") in Figure 1c shows a peak shift assigned to Pt_3Si, consistent with the diffraction behavior in Figure 1a (bottom-right quadrant). Quantitative analysis (Figure 1c, insets) determined that this sample consists of 74% Pt_3Si and 26% metallic Pt. Figure 1c also shows the high-resolution XPS spectra of the annealed Pt:*a*-Si=1:1 sample ("Pt_2Si Sample"). Quantitative XPS analysis showed that this sample consists of 70% Pt_2Si phase, while the remaining 30% are a mixture between metallic Pt, Pt_3Si and PtSi (7% Pt, 14% Pt_3Si, 9% PtSi). The high-resolution XPS spectra of the annealed Pt:*a*-Si=1:3 sample ("PtSi Sample") is displayed in Figure 1c. This sample is composed of 92% PtSi phase (remainder: 2% Pt, 1% Pt_3Si, 5% Pt_2Si), which matches well with the PtSi diffraction pattern in Figure 1a (left-top quadrant). The quantitative XPS analysis confirmed the Pt_xSi stoichiometries determined using *in situ* TEM electron diffraction. The overall results confirm that the stoichiometry of Pt_xSi thin films can be precisely tuned using source-controlled solid-state diffusion.

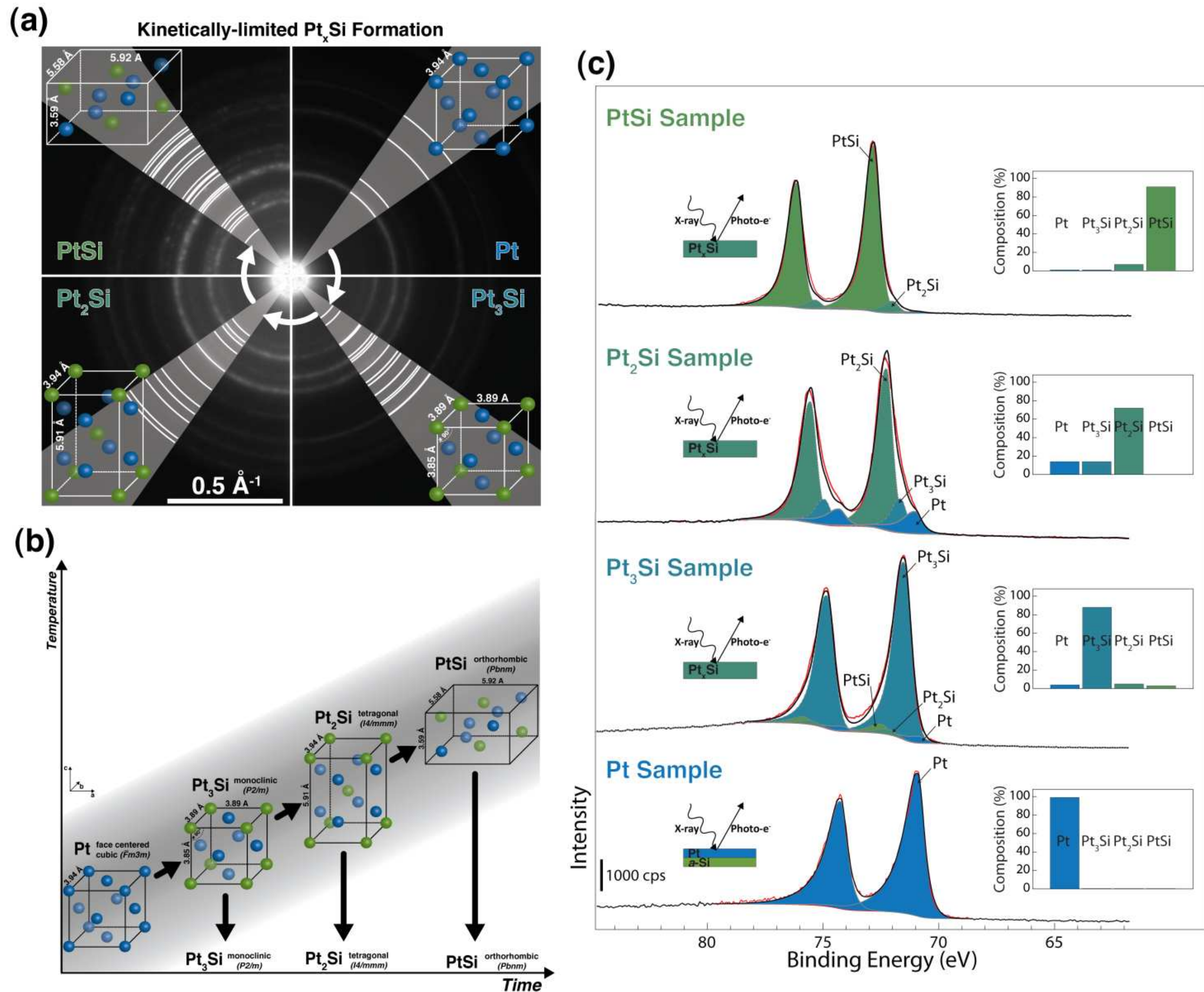

Figure 2. Kinetically-limited Pt_xSi formation. a, Electron diffraction pattern of as-deposited Pt and Pt_3Si, Pt_2Si, and PtSi films produced using kinetically-limited solid-state diffusion. Grey slices indicate diffraction ring positions according to the theoretical crystal structure shown schematically for each phase. b, Schematic of the kinetically-limited solid-state diffusion process which utilizes precise control of the temperature-time regime to obtain the desired Pt_xSi phase. c, High-resolution XPS spectra of the Pt f peaks for as-deposited Pt and resulting Pt_xSi formed on TEM grids using kinetically-limited solid-state diffusion. *PtSi sample* (Pt:*a*-Si=1:3): quantitative analysis indicates formation of 91% of PtSi. *Pt_2Si sample* (Pt:*a*-Si=1:1): quantitative analysis indicates formation of 72% Pt_2Si. *Pt_3Si sample* (Pt:*a*-Si=2:1): quantitative analysis indicates formation of 88% Pt_3Si. *Pt sample:* quantitative analysis indicates the presence of pure metallic Pt.

3.2 Kinetically-limited solid-state diffusion

Samples with Pt:*a*-Si thickness ratio of 1:3 were produced to test if precise control of the temperature-time regime during silicidation can be used to tune the Pt_xSi stoichiometry (*i.e.* kinetically-limited solid-state diffusion). This Pt:*a*-Si thickness ratio will ultimately lead to PtSi formation, while passing the Pt_3Si and Pt_2Si stoichiometries (as seen in Figure 1b). Figure 2 summarizes the results. Figure 2a shows SAD electron diffraction images recorded at room temperature and after the annealing process has been halted at specific temperatures to produce highly selective Pt_xSi phases. The as-deposited sample, which exhibited a Pt electron diffraction pattern (top-tight quadrant, Figure 2a), was heated up to 200 °C to form Pt_3Si and then quickly cooled down to retain this phase at room temperature (bottom-right quadrant). The Pt_3Si film was subsequently heated up to 300 °C to form Pt_2Si and quickly cooled down to retain this phase at room temperature (bottom-left quadrant). Finally, the formed Pt_2Si film was heated up to 500 °C so that PtSi is formed and subsequently cooled down (top-left quadrant).

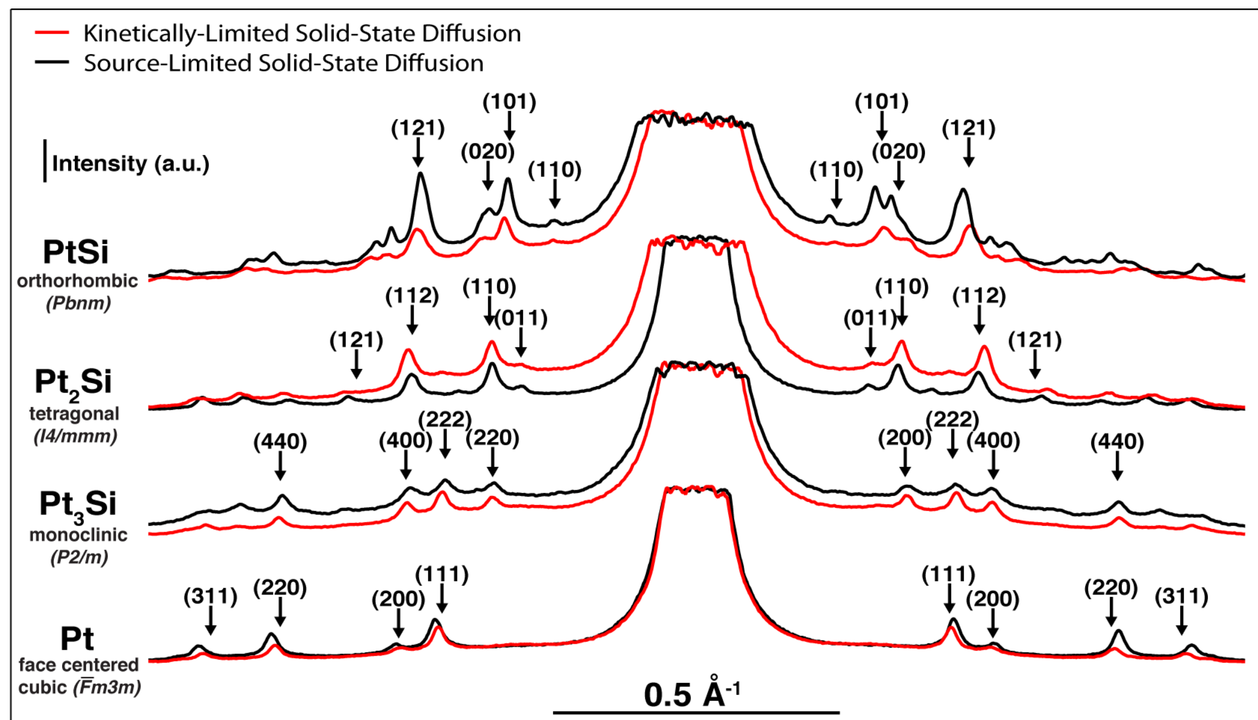

Figure 3. Comparison of diffraction pattern intensity distributions obtained from the kinetically-limited and source-limited solid-state diffusion samples. Peak locations and intensity ratios are similar for both methods and indicate that the two methods produce similar Pt_xSi compositions. The theoretical peak positions of the four strongest peaks are indicated by the downward arrows.

The annealed TEM grid was characterized using XPS to determine the stoichiometry of the Pt_xSi phases formed (Figure 2c). The results presented indicate a similar phase selectivity for kinetically-limited diffusion (88% Pt_3Si, 72 % Pt_2Si, 91% PtSi) and for the source-limited case (74% Pt_3Si, 70% Pt_2Si, 92% PtSi). Comparison of the kinetically-limited diffraction patterns (Figure 2a) with those from the source-limited experiments (Figure 1a) show that the peak positions and intensity ratios are similar (Figure 3), which confirms the similar composition of the Pt_xSi phases for kinetically-limited and source-limited experiments measured using XPS. Figure 2a also shows that all phases formed exhibit minimal grain growth. Dark-field TEM results also indicated that the formed Pt_xSi films are nanocrystalline. Figure 2b summarizes the kinetically-limited Pt_xSi formation experiments, and shows that the stoichiometry of Pt_xSi films was precisely tunable by controlling the temperature-time regime during the annealing. The *in situ* TEM experiments presented in Figure 2 prove that kinetically-controlled solid-state diffusion is a highly effective way to tune the Pt_xSi stoichiometry.

3.3 Specifics of Pt_3Si formation

Both source-limited and kinetically-limited solid-state diffusion experiments (Figure 1, Figure 2) were able to produce highly selective Pt_3Si films, which have not been experimentally reported before or observed during Pt/sc-Si experiments. The well-studied Pt/*sc*-Si system is characterized by the specific Pt_xSi formation sequence of Pt diffusing into *sc*-Si around 250-300 °C to form the intermediate Pt_2Si phase. After all Pt is consumed, *sc*-Si will diffuse into Pt_2Si at 300-450 °C to form the thermodynamically stable PtSi phase.[27,28] We propose that the amorphous nature of the *a*-Si film used in our experiments alters the diffusion behavior compared to *sc*-Si, which leads to the formation of the Pt_3Si phase. The Pt_3Si phase is formed due to the fact that in the Pt/*a*-Si system, *a*-Si acts initially as the dominant diffusing species (DDS) in contrast to the Pt/sc-Si system where Pt is initially the DDS. The distribution of bonding characteristics of *a*-Si compared to *sc*-Si leads to reduced activation energies for *a*-Si self-diffusion of up to 27% compared to those for *sc*-Si.[29] Thus, *a*-Si becomes mobile at lower temperatures than *sc*-Si. In addition to the increased mobility of *a*-Si, the Pt diffusivity is drastically reduced in *a*-Si compared to *sc*-Si. Pt has a diffusion coefficient at 500 °C of $\sim 5 \times 10^{-18}$ m^2/s in *a*-Si,[30] whereas the diffusion coefficient of Pt in *sc*-Si is $\sim 5 \times 10^{-16}$ m^2/s,[31] which means that Pt diffuses two orders of magnitude faster in *sc*-Si than in *a*-Si. Both the increased *a*-Si and reduced Pt diffusivity contribute to the *a*-Si diffusion into Pt and subsequent formation of Pt_3Si for the Pt/*a*-Si system.

The observed Pt_3Si formation can also be understood by the high degree of resemblance between the Pt and Pt_3Si crystal structures, including the lattice parameter. The Pt_3Si unit cell can be imagined as a Pt unit cell with the corner atoms replaced by Si. The ease of transformation between Pt and Pt_3Si without the need for massive atomic restructuring is thought to be the reason for such low temperature metamorphosis.

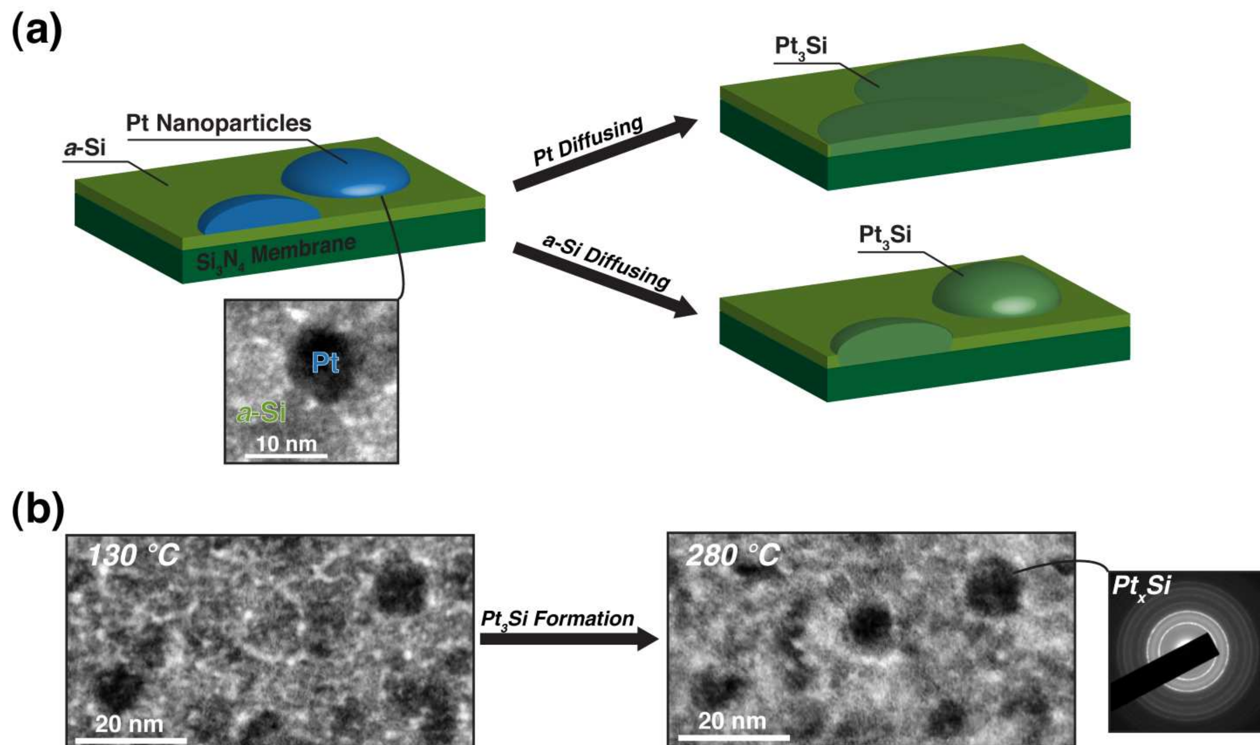

Figure 4. Determination of the dominant diffusing species (DDS) during Pt_3Si formation. a, The schematic and the TEM image on the left shows the as-deposited sample: an *a*-Si film covered by Pt nanoparticles. Annealing will lead to Pt_3Si formation. If Pt is the DDS, then the Pt nanoparticles will completely diffuse into the underlying *a*-Si layer and the Pt-containing region (high Z contrast) will appear larger in TEM images. If Si is the DDS, then the nanoparticle shape and size will be nearly preserved and no major change of the high Z contrast region will be visible in the TEM. b, TEM images of several Pt nanoparticles before (at 130 °C) and after (280 °C) Pt_3Si formation. The overall shape and size of the Pt and Pt_3Si nanoparticles is similar, indicating that Pt_3Si formation occurs through diffusion of *a*-Si into Pt. The electron diffraction pattern shows that Pt_3Si particles were formed.

To demonstrate that *a*-Si is the diffusing species instead of Pt and that this leads to Pt_3Si formation, we coated a Si_3N_4-support TEM grid with *a*-Si and, subsequently, with Pt nanoparticles of ~10 nm diameter (as shown in Figure 4a). Figure 4a shows a schematic and TEM image of the as-deposited sample together with the theoretical pathways leading to the formation of Pt_3Si, *i.e.*, the diffusion of Pt in *a*-Si or the diffusion of *a*-Si in Pt. If Pt is the DDS, then the Pt nanoparticles will diffuse into the underlying *a*-Si layer and a TEM Z-contrast image will show significant broadening of the Pt-containing regions. If, on the other hand, *a*-Si is the diffusing species as proposed here, then the general shape of the Pt nanoparticles should be conserved during Pt_3Si formation as only a small amount of *a*-Si is diffusing into the nanoparticles. Figure 4b shows an area of the sample with several Pt nanoparticles before (at 130 °C) and after (at 280 °C) Pt_3Si formation. The overall shape and size of the nanoparticles do not undergo any significant changes due to Pt_3Si formation. This result confirms that *a*-Si is the DDS, and that it diffuses into Pt to form Pt_3Si, which means that the occurrence of Pt_3Si in *a*-Si-based silicidation experiments is entirely due to the high diffusivity of *a*-Si, and that such films are not attainable using *sc*-Si.

The Pt_3Si films resulting from Pt/*a*-Si annealing have several advantages over PtSi films that result from Pt/*sc*-Si. Most notably, Pt_3Si possesses similar mechanical properties as PtSi (~50% greater hardness and modulus compared to Pt),[10] but with a higher electrical conductivity.[10,11] The increased hardness of Pt_3Si can also be understood from our source-limited heating experiments where we observe not only grain coarsening but also formation of anti-phase boundaries (APBs) (Supporting Information Figure S2), which are two dimensional defects commonly found in $L1_2$ type crystal structures.[32-35] These APBs will hinder dislocation motion and thereby plastic deformation.

4. CONCLUSIONS

In summary, we present two routes to control and predetermine the stoichiometry, crystal structure and thereby the properties of thin Pt_xSi films. Both the precise control of the precursor film thicknesses (source-limited solid-state diffusion) and the precise control of the temperature-time regime during silicidation (kinetically-limited solid-state diffusion) were able to produce highly selective Pt_3Si, Pt_2Si, and PtSi films. These two routes to adjust the silicide stoichiometry, crystal structure and properties will also be applicable to other metal silicides (*e.g.* Ti, Ni, W, Co, Mo, and Cr silicides) and may give access to phases not attainable using traditional formation routes. We also show that the diffusion mechanism during Pt_xSi formation using Pt/*a*-Si bilayers significantly differs from the well-studied Pt/*sc*-Si system, allowing the formation of Pt_3Si - a stoichi-

ometry with significant potential as an electrical conductive and wear-resistive coating.

ASSOCIATED CONTENT

Supporting Information. Schematics of the experimental procedure and TEM images of the anti-phase boundaries found in Pt_3Si can be found in the supporting information. This material is available free of charge via the Internet at http://pubs.acs.org.

AUTHOR INFORMATION

Corresponding Author

*E-mail: carpick@seas.upenn.edu

Present Addresses

‖Laboratoire de Tribologie et Dynamique des Systèmes, Ecole Centrale de Lyon, 35 Avenue Guy de Collongue, Ecully, 69134 France.

Author Contributions

All authors have given approval to the final version of the manuscript. § These authors contributed equally.

Notes

The authors declare no competing financial interest.

ACKNOWLEDGMENT

The authors acknowledge the use of instrumentation from the Nano/Bio Interface Center (NBIC) and the Nanoscale Characterization Facility (NCF) at the University of Pennsylvania. Funding from the DMREF program of the National Science Foundation (award number: CMMI-1334241) is acknowledged. F.M. acknowledges support from the Marie Curie International Outgoing Fellowship for Career Development within the 7th European Community Framework Program under contract no. PIOF-GA-2012-328776.

REFERENCES

(1) Miglio, L.; d'Heurle, F. *Silicides - Fundamentals and Applications;* World Scientific Publishing: Singapore, 2000.
(2) Peter, A. P.; Meersschaut, J.; Richard, O.; Moussa, A.; Steenbergen, J.; Schaekers, M.; Tokei, Z.; Van Elshocht, S.; Adelmann, C. *Chem. Mater.* 2015, *27*, 245-254.
(3) Tu, K. N.; Thompson, R. D.; Tsaur, B. Y. *Applied Physics Letters* 1981, *38*, 626-628.
(4) Rhoderick, E. H.; Williams, R. H. *Metal-Semiconductor Contacts,* Clarendon Press: Oxford, 1988.
(5) Chen, L. J. *JOM* 2005, *57*, 24-31.
(6) Rowe, D. M. *Thermoelectrics Handbook: Macro to Nano*, Taylor & Francis Group: Abingdon, 2006.
(7) Fedoriv, M. I. *J. Thermoelectr.* 2009, *2*, 51-60.
(8) Itoh, T.; Yamada, M. *J. Electron. Mater.* 2009, *38*, 925-929.
(9) de Boor, J.; Dasgupta, T.; Kolb, H.; Compere, C.; Kelm, K.; Mueller, E. *Acta Mater.* 2014, 77, 68-75.
(10) Streller, F.; Wabiszewski, G. W.; Mangolini, F.; Feng, G.; Carpick, R. W. *Adv. Mater. Interfaces* 2014, *1,* 1300120.
(11) Streller, F.; Wabiszewski, G. E.; Carpick, R. W. *IEEE Nanotechnol. Mag.*, DOI: 10.11109/MNANO.2014.2373451.
(12) Loh, O. Y.; Espinosa, H. D. *Nat. Nanotechnol.* 2012, 7, 283-295.
(13) Naik, G. V.; Shalaev, V. M.; Boltasseva, A. *Adv. Mater.* 2013, *25*, 3264-3294.
(14) Liu, C; Li, F.; Ma, L.-P.; Cheng, H.-M. *Adv. Mater.* 2010, 22, E28-E62.
(15) Lin, H.-K.; Cheng, H.-A; Lee, C.-Y.; Chiu, H.-T. *Chem. Mater.* 2009, *21*, 5388-5396.
(16) Li, H.; Wu, J.; Wang, Z. M. *Silicon-based Nanomaterials*, Springer: Berlin, 2013.
(17) Higgins, J. M.; Ding, R.; Jin, S. *Chem. Mater.* 2011, *23*, 3848-3853.
(18) Schmitt, A. L.; Higgins, J. M.; Szczech, J. R.; Jin, S. J. Mater. Chem. 2010, *20*, 223-235.
(19) Chou, Y.-C.; Wu, W.-W.; Cheng, S.-L.; Yoo, B.-Y.; Myung, N.; Chen, L. J.; Tu, K. N. *Nano Lett.* 2008, *8*, 2194-2199.
(20) Liu, X. H.; Wang, J. W.; Huang, S.; Fan, F.; Huang, X.; Liu, Y.; Krylyk, S.; Yoo, J.; Dayeh, S. A.; Davydov, A. V.; Mao, S. C.; Picraux, T.; Zhang, S.; Li, J.; Zhy, T.; Huang, J. Y. *Nat. Nanotechnol.* 2012, *7*, 749-756.
(21) Lin, Y.-C.; Chen, Y.; Xu, D.; Huang, Y. *Nano Lett.* 2010, *10*, 4721-4726.
(22) Stach, E. A.; Pauzauskie, P. J.; Kuykendall, T.; Goldberger, J.; He, R.; Yang, P. *Nano Lett.* 2003, *3*, 867-869.
(23) Nukala, P.; Agarwal, R.; Qian, X.; Jang, M. H.; Dhara, S.; Kumar, K.; Johnson, A. T. C.; Li, J.; Agarwal, R. *Nano Lett.* 2014, *14*, 2201-2209.
(24) Mangolini, F.; Ahlund, J.; Wabiszewski, G. E.; Adiga, V. P.; Egberts, P.; Streller, F.; Backlund, K.; Karlsson, P. G.; Wannberg, B.; Carpick, R. W. *Rev. Sci. Instrum.* 2012, *83*, 093112.
(25) Mangolini, F.; Rossi, A.; Spencer, N. D. *J. Phys. Chem. C* 2011, *115*, 1339-1354.
(26) Tanuma, S. Surface Analysis by Auger and X-Ray Photoelectron Spectroscopy, IM Publications: Charlton, 2003.
(27) Stark, T.; Gruenleitner, H.; Hundhausen, M.; Ley, L. *Thin Solid Films* 2000, *358*, 73-79.
(28) Poate, J. M.; Tisone, T. C. *Appl. Phys. Lett.* 1974, *24*, 391-393.
(29) Kobayashi, T.; Koguchi, M.; Iijima, S.; Ohkura, M. *J. Electrochem. Soc.* 1994, *141*, 1365-1369.
(30) Coffa, S.; Poate, J. M.; Jacobson, D. C. *Phys. Rev. B* 1992, *45*, 8355-8358.
(31) Lerch, W.; Stolwijk, N. A.; Mehrer, H.; Poisson, C. *Semicond. Sci. Technol.* 1995, *10*, 1257-1263.
(32) Tichelaar, F. D.; Schapink, F. W. *Philos. Mag. A* 1986, *54*, 55-60.
(33) Tichelaar, F. D.; Schapink, F. W. *J. Phys. Colloq.* 1988, *49*, 293-298.
(34) Janowski, G. M.; Stafford, G. R. *Metall. Trans. A* 1992, *23*, 2715-2723.
(35) Chou, T. C.; Chou, Y. T. *MTS Proceedings* 1984, *39*, 461-474.

Insert Table of Contents artwork here